Supporting Information for the article

Biocompatible Phosphorescent Ir(III) Oxygen Sensor Functionalized with Oligo(ethylene glycol) Groups: Synthesis, Photophysics and Application in PLIM Experiments

to be published in New Journal of Chemistry

Ilya S. Kritchenkov[1], Anastasiia A. Elistratova,[1] Viktor V. Sokolov[1], Pavel S. Chelushkin[1], Marina V. Shirmanova[2], Maria M. Lukina[2], Varvara V. Dudenkova[2], Vladislav I. Shcheslavskiy[3], Sviatlana Kalinina[4], Kirsten Reeß[4], Angelika Rück[4], Sergey P. Tunik[1]*

[1] *Saint-Petersburg State University, Institute of Chemistry, Universitetskii pr., 26, 198504 St. Petersburg, Russia.*

[2] *Privolzhskiy Research Medical University, Institute of Experimental Oncology and Biomedical Technologies, Minin and Pozharsky Sq., 10/1, 603005 Nizhny Novgorod, Russia.*

[3] *Becker&Hickl GmbH, Nunsdorfer Ring 7-9, 12277 Berlin, Germany.*

[4] *University Ulm, Core Facility Confocal and Multiphoton Microscopy, N24, Albert Einstein Allee 11, 89081 Ulm, Germany.*

** E-mail: sergey.tunik@spbu.ru*

NMR spectroscopy and ESI mass-spectrometry data

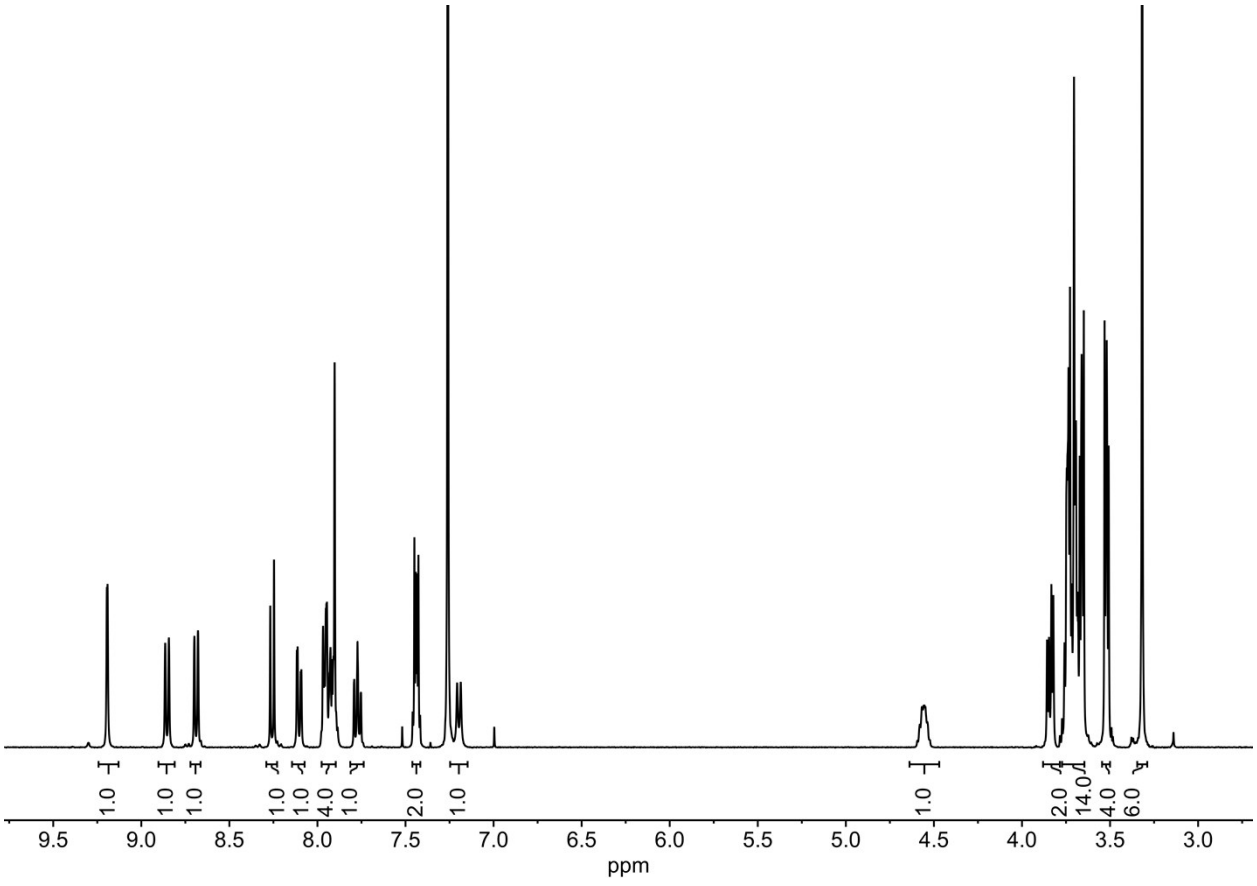

Figure S1. ^{1}H NMR spectrum of **N^C2**, $CDCl_3$, 298 K.

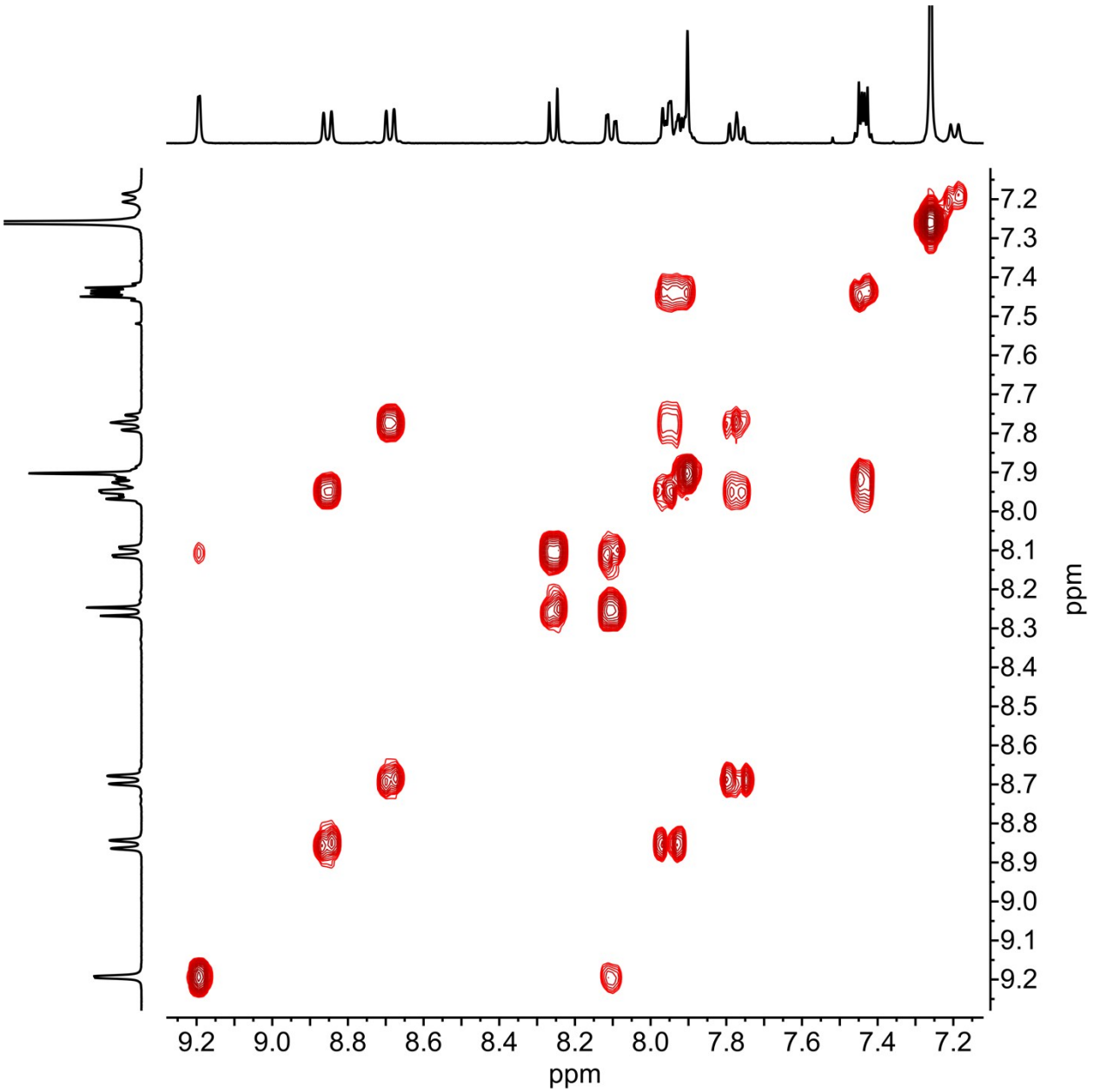

Figure S2. ^{1}H-^{1}H COSY NMR spectrum of **N^C2**, $CDCl_3$, 298 K.

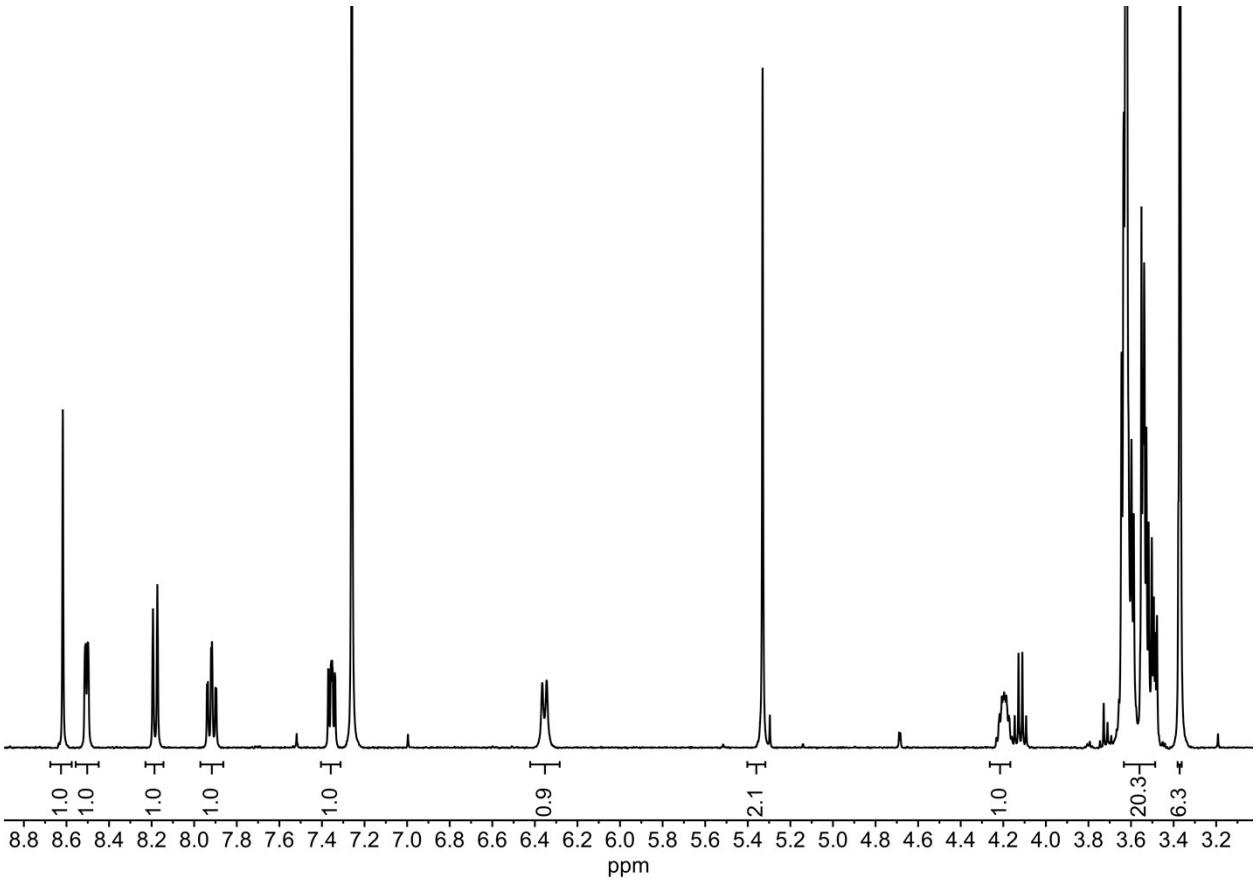

Figure S3. ^{1}H NMR spectrum of **N^N2**, $CDCl_3$, 298 K.

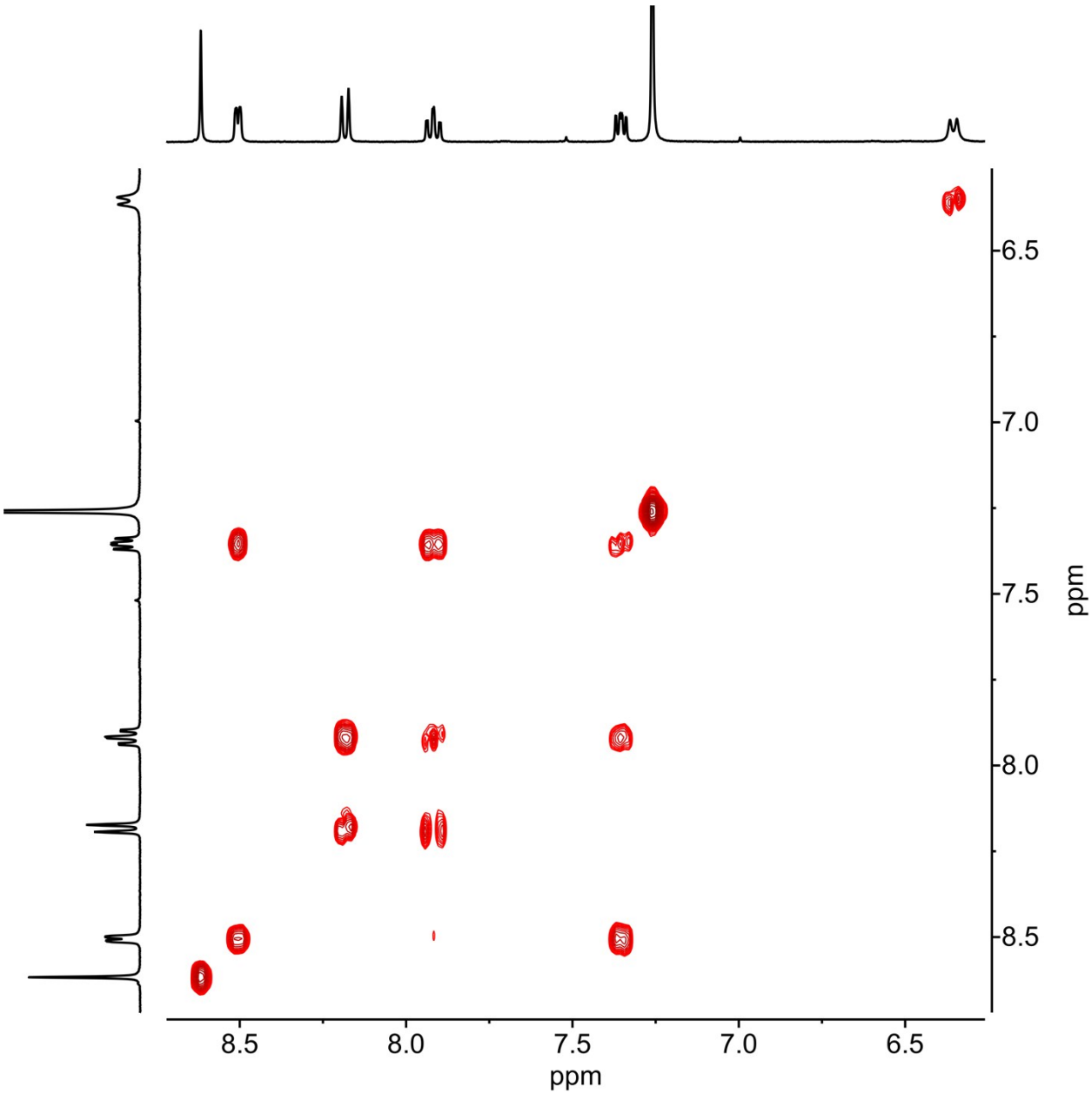

Figure S4. ^{1}H-^{1}H COSY NMR spectrum of **N^N2**, $CDCl_3$, 298 K.

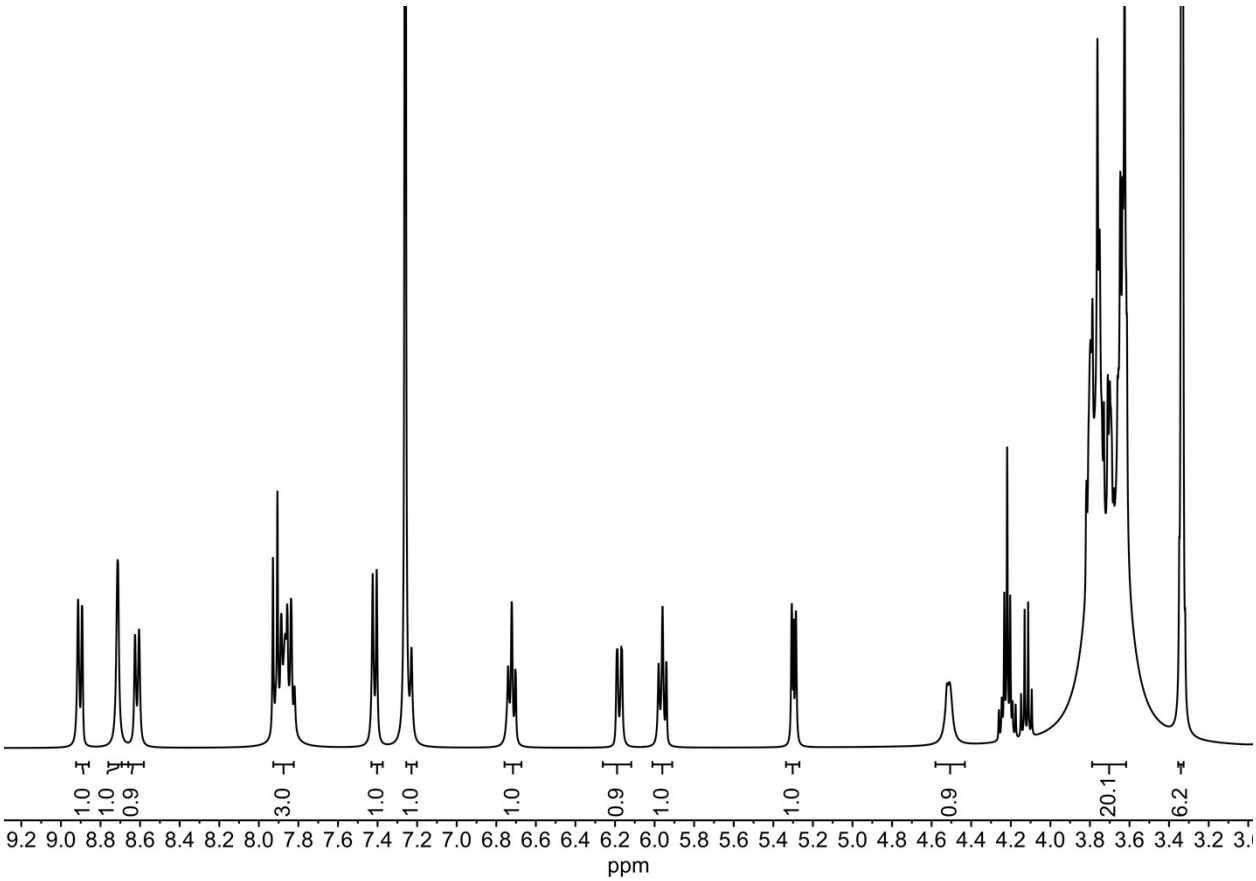

Figure S5. ^{1}H NMR spectrum of $\mathbf{Ir_2(N\hat{}C2)_4Cl_2}$, $CDCl_3$, 298 K.

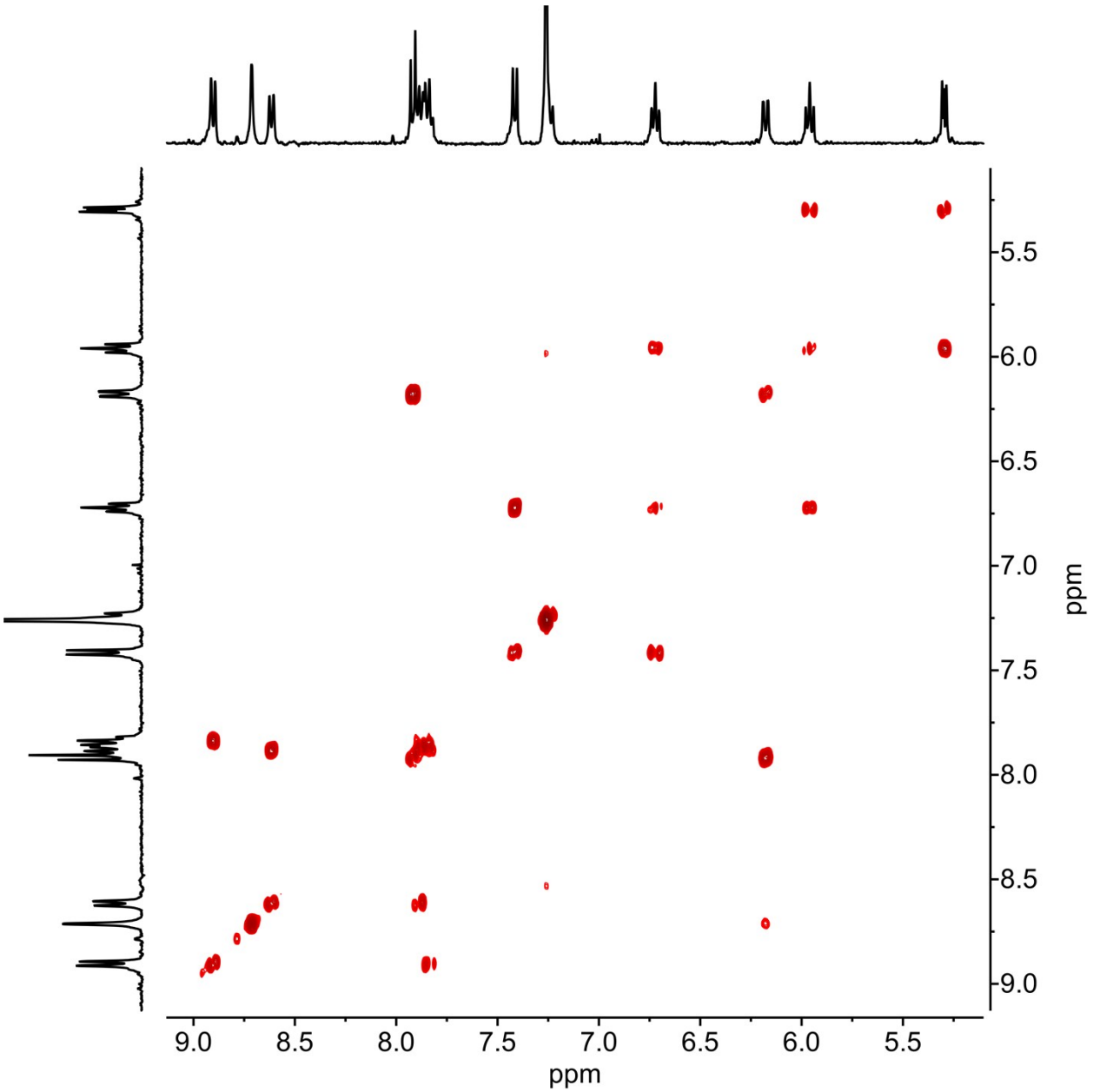

Figure S6. ^{1}H-^{1}H COSY NMR spectrum of **Ir_2(N^C2)$_4$$Cl_2$**, $CDCl_3$, 298 K.

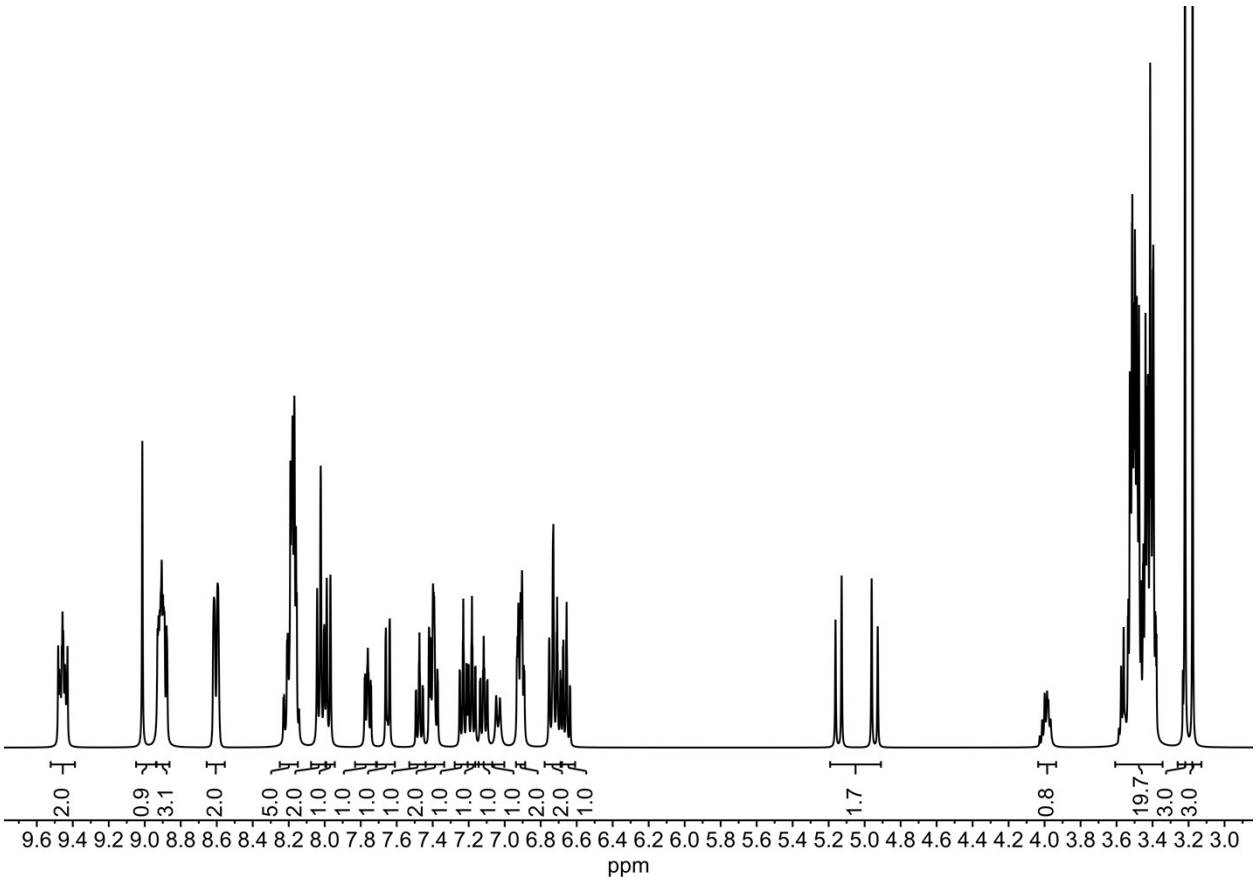

Figure S7. ^{1}H NMR spectrum of **1**, $(CD_3)_2CO$, 298 K.

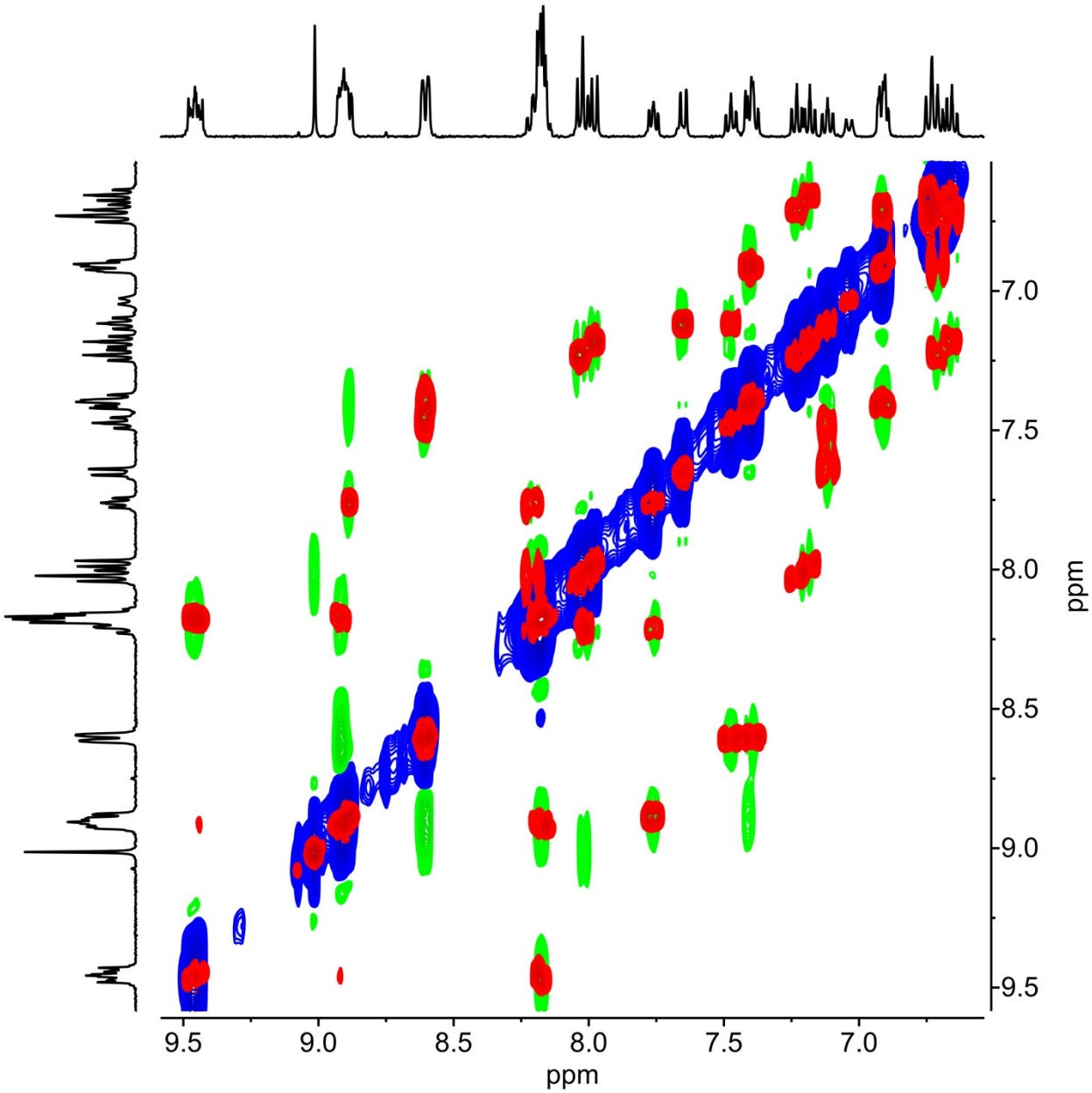

Figure S8. ^{1}H-^{1}H COSY and NOESY NMR spectra of **1**, $(CD_3)_2CO$, 298 K. Red diagonal and crosspeaks are from COSY spectrum, blue diagonal and green crosspeaks are from NOESY spectrum.

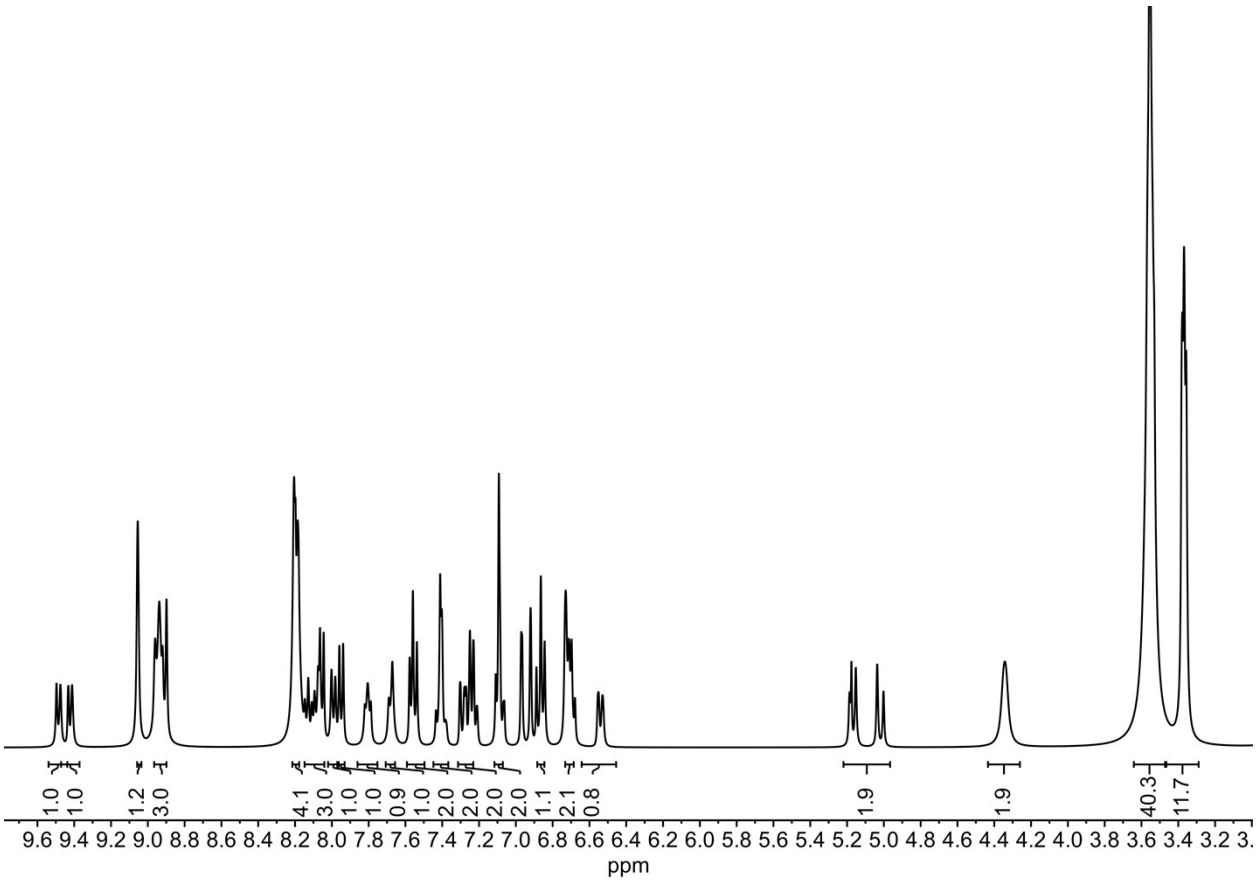

Figure S9. ^{1}H NMR spectrum of **2**, $(CD_3)_2CO$, 298 K.

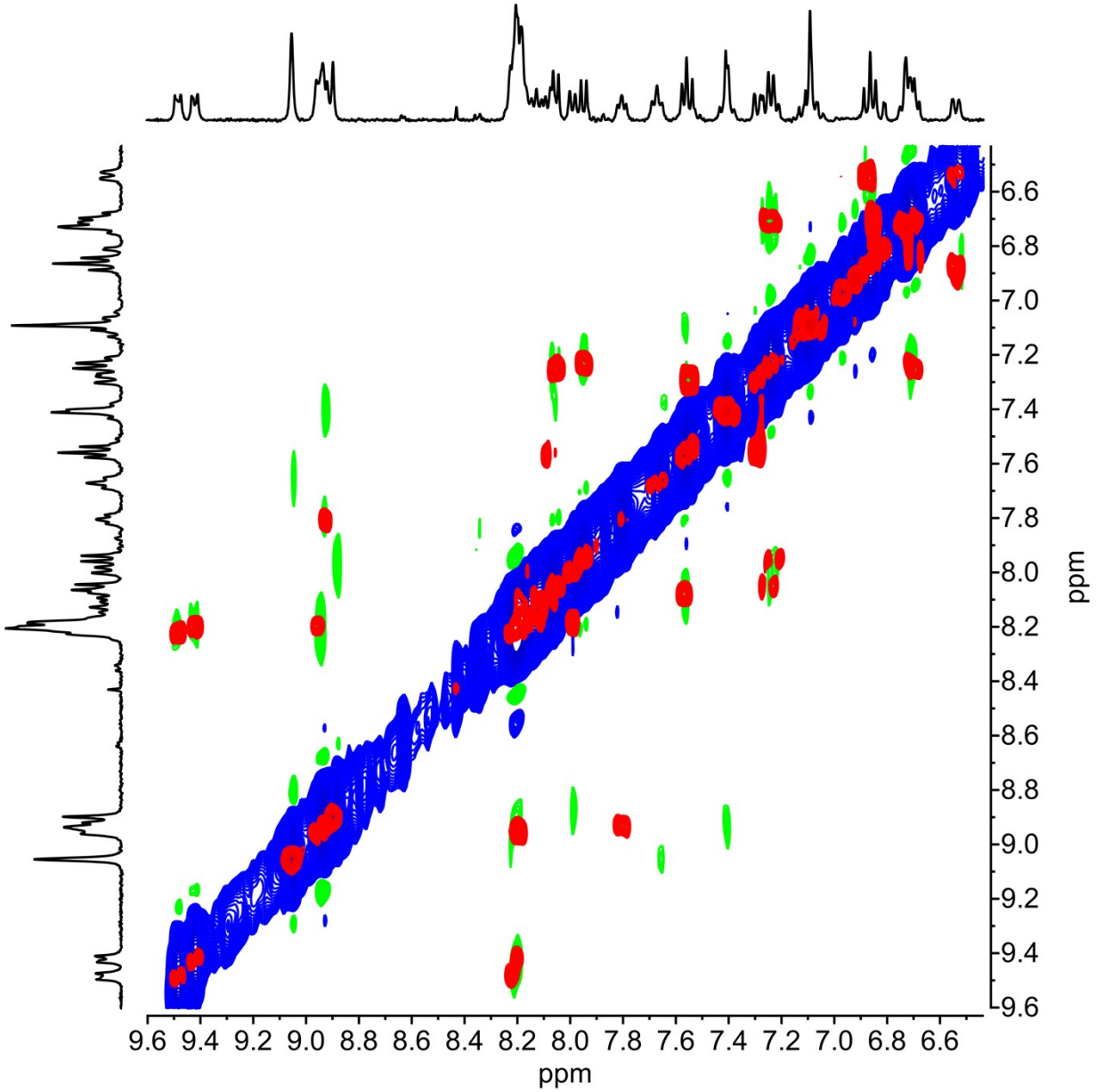

Figure S10. ^{1}H-^{1}H COSY and NOESY NMR spectra of **2**, $(CD_3)_2CO$, 298 K. Red diagonal and crosspeaks are from COSY spectrum, blue diagonal and green crosspeaks are from NOESY spectrum.

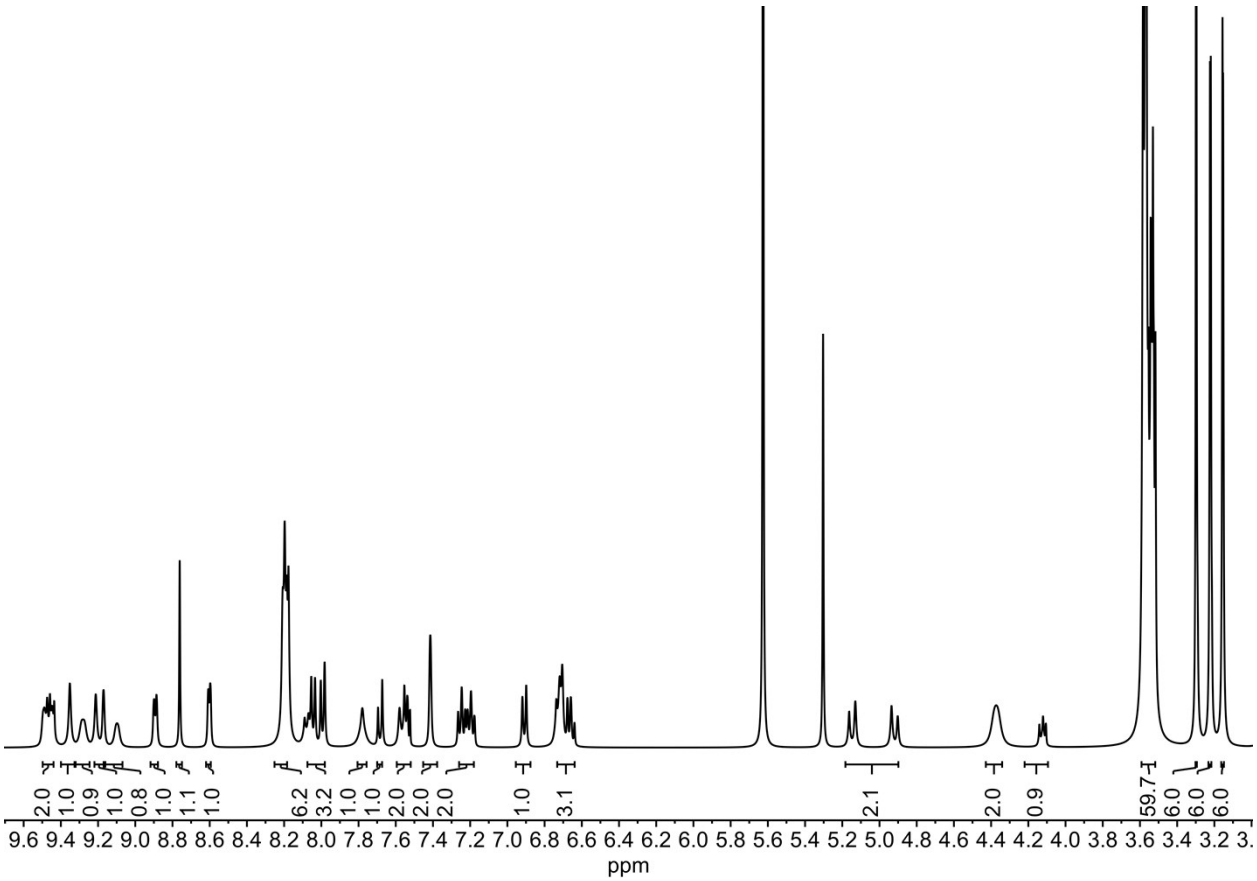

Figure S11. ^{1}H NMR spectrum of **3**, $(CD_3)_2CO$, 298 K.

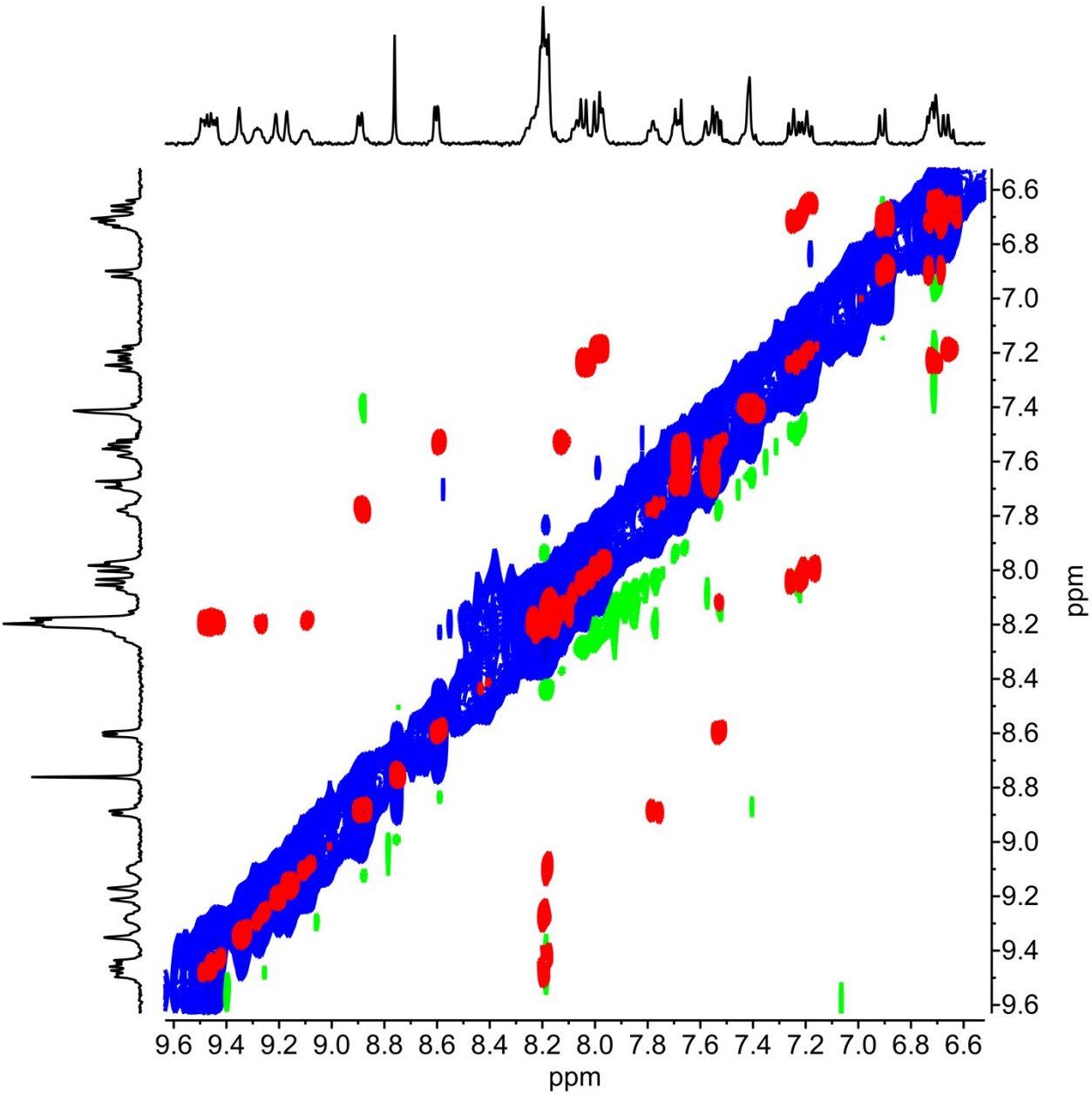

Figure S12. ^{1}H-^{1}H COSY and NOESY NMR spectra of **3**, $(CD_3)_2CO$, 298 K. Red diagonal and crosspeaks are from COSY spectrum, blue diagonal and green crosspeaks are from NOESY spectrum (quality of NOESY spectrum is poor due to high molecular mass of the compound).

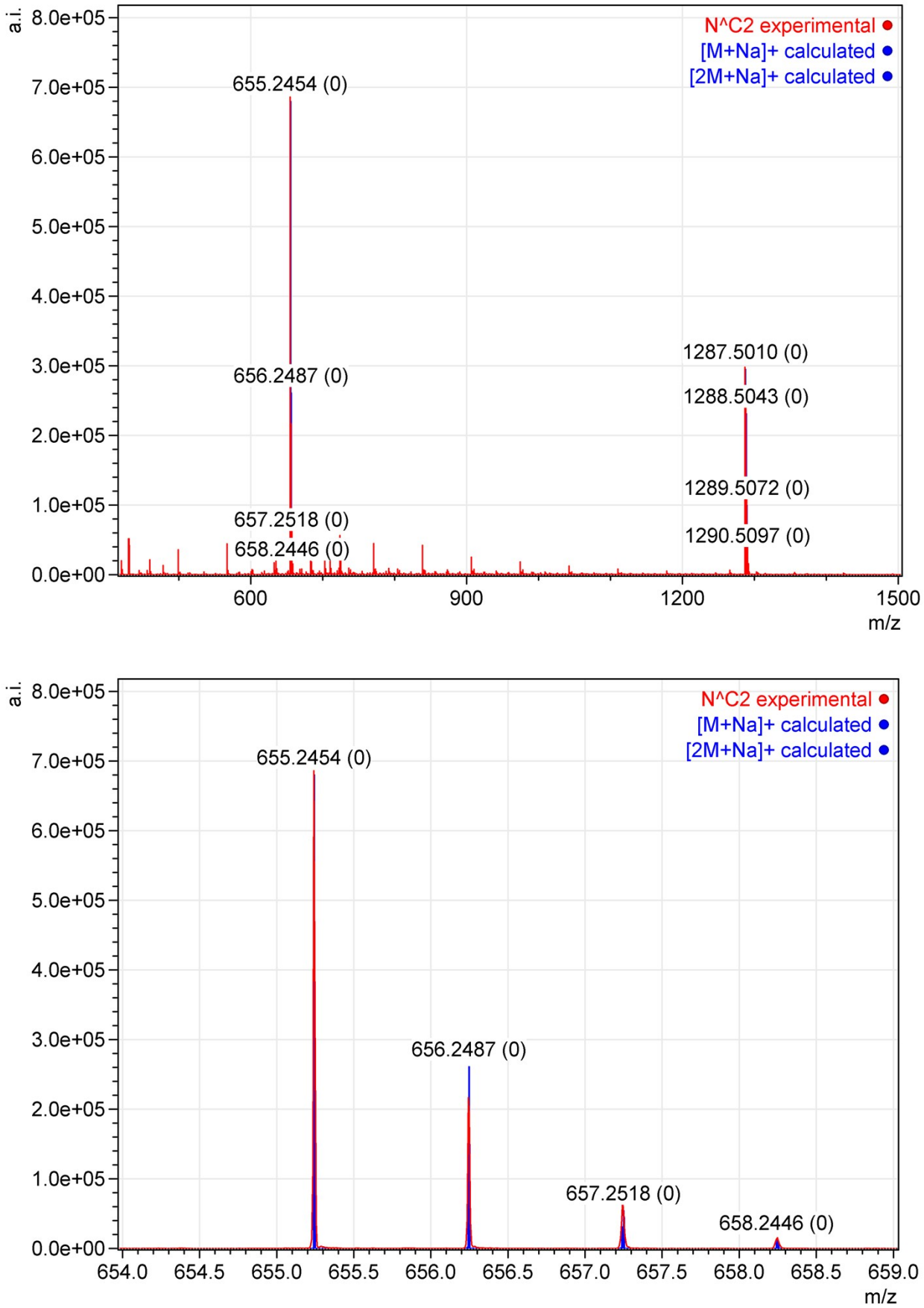

Figure S13. ESI$^+$ mass-spectrum of **N^C2** (full view and [M+Na]$^+$ cation area), solvent – methanol.

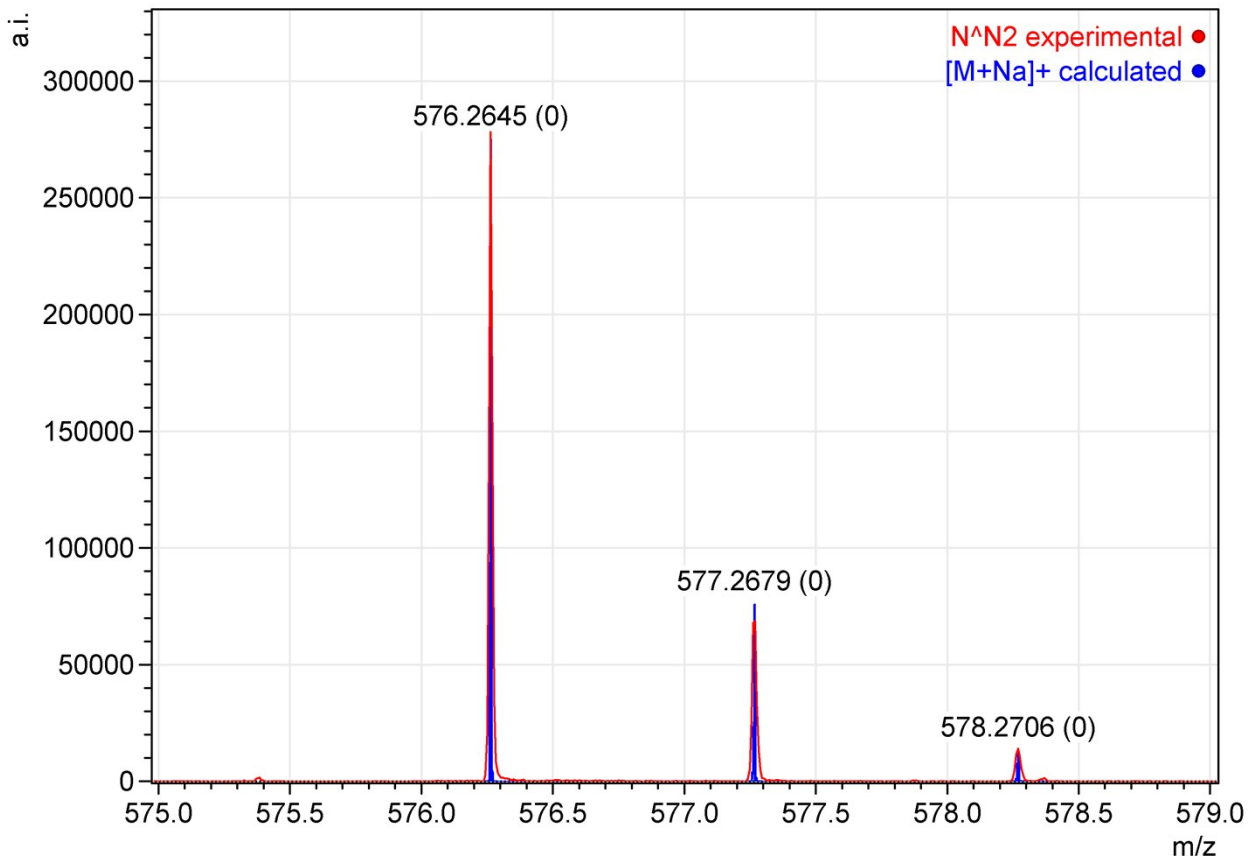

Figure S14. ESI$^+$ mass-spectrum of **N^N2** ([M+Na]$^+$ cation area), solvent – methanol.

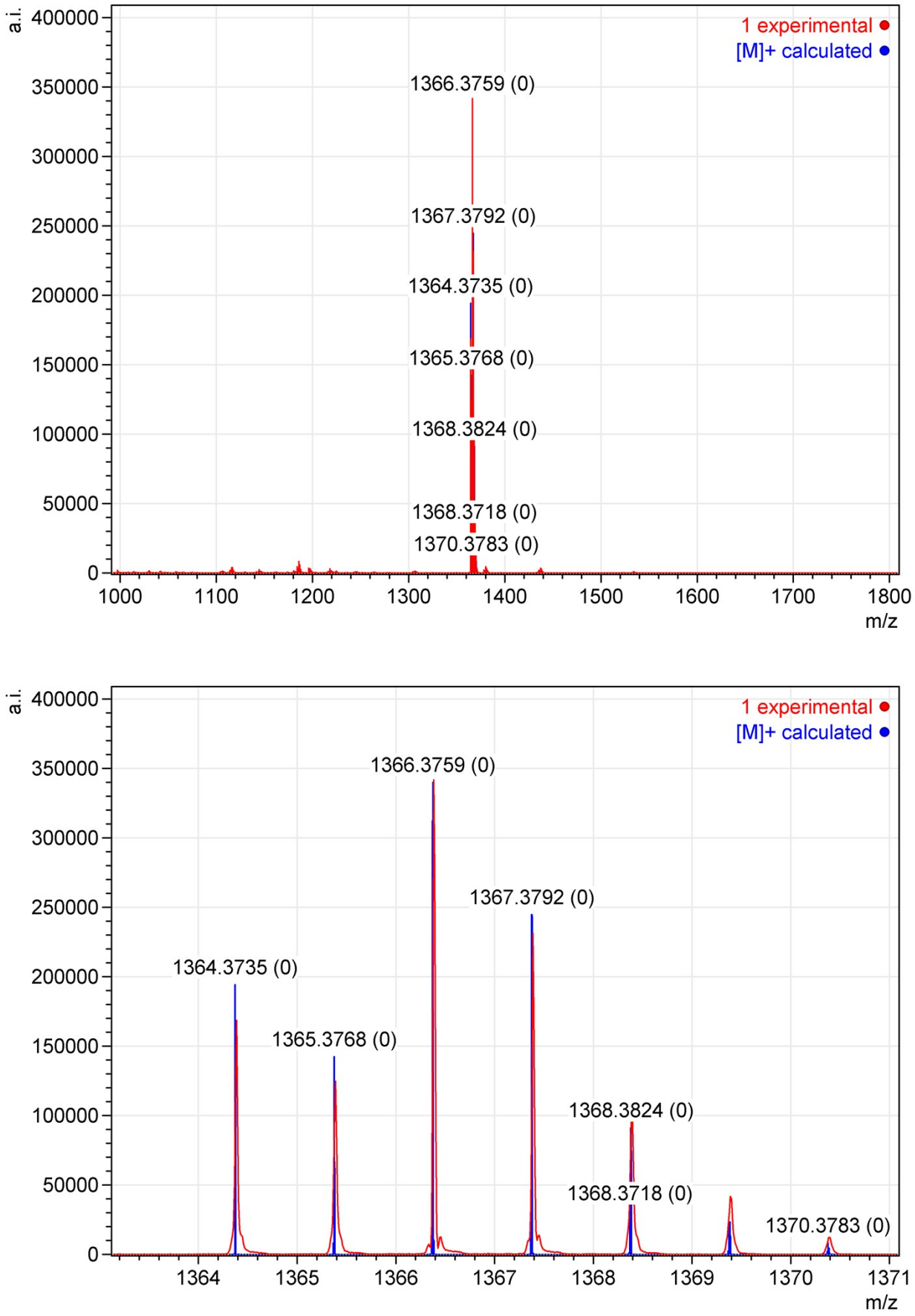

Figure S15. ESI$^+$ mass-spectrum of **1** (full view and $[M]^+$ cation area), solvent – methanol.

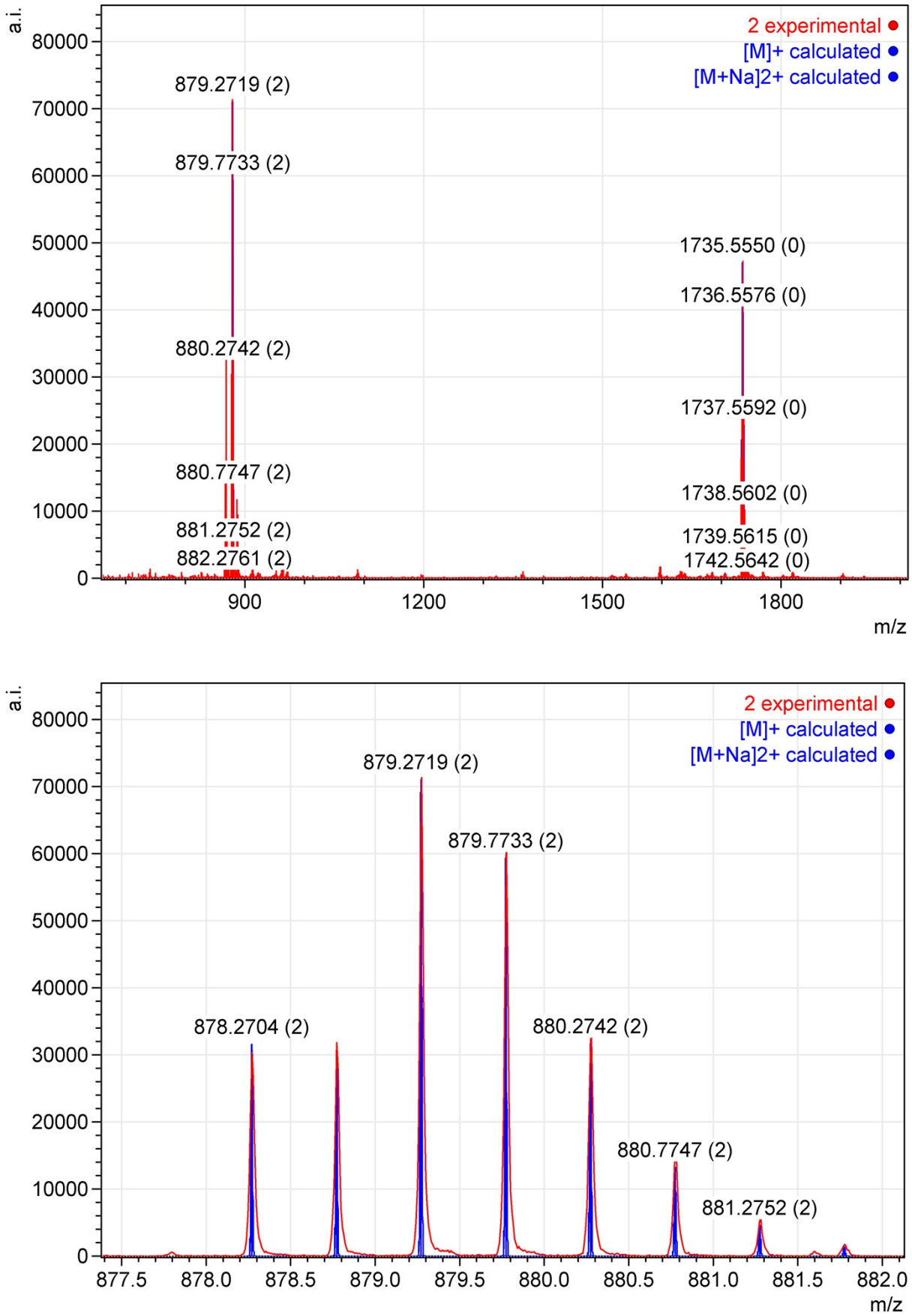

Figure S16. ESI^+ mass-spectrum of **2** (full view and $[M+Na]^{2+}$ cation area), solvent – methanol.

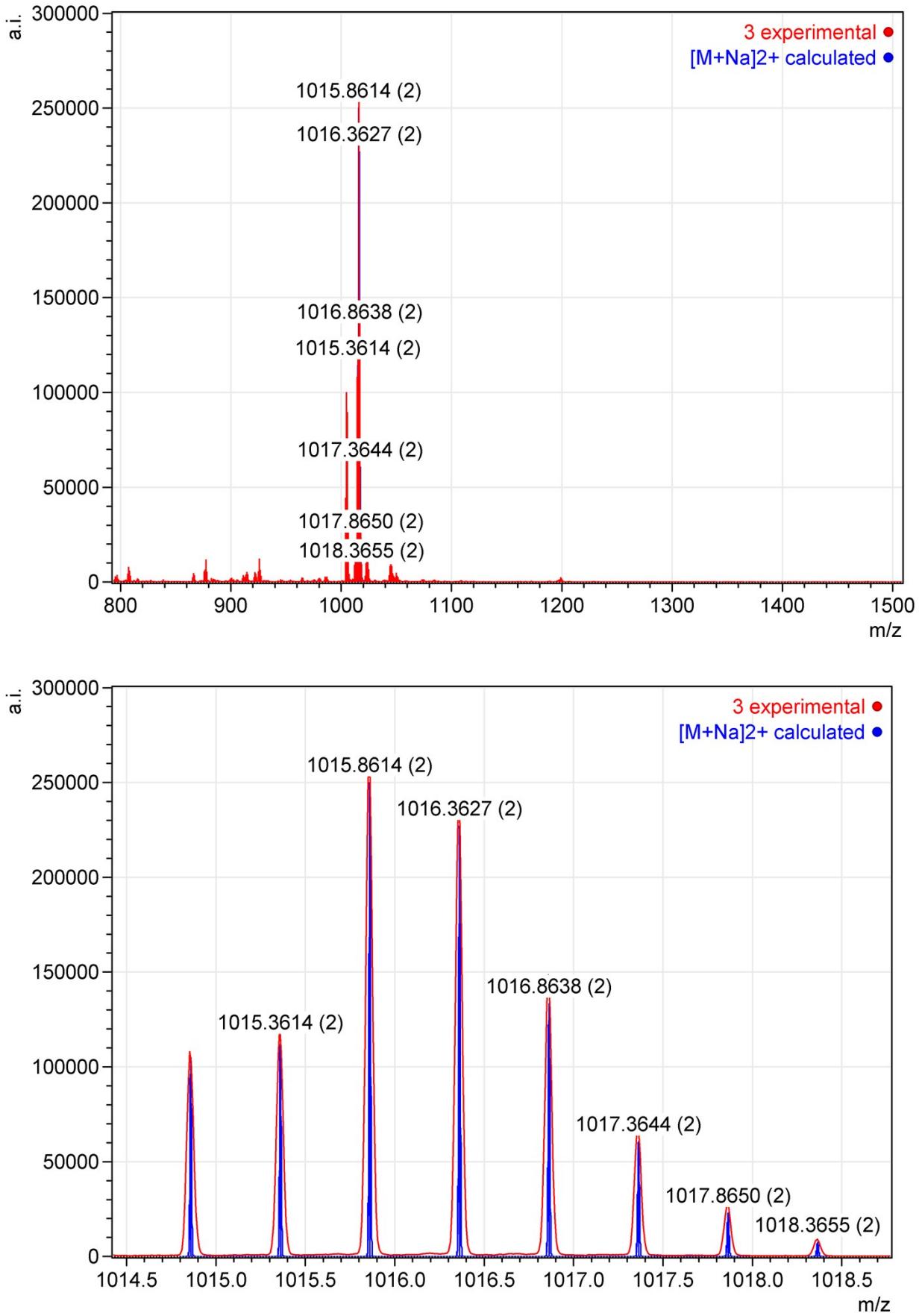

Figure S17. ESI^{+} mass-spectrum of **3** (full view and [M+Na]$^{2+}$ cation area), solvent – methanol.

Photophysical data for complexes 1-3

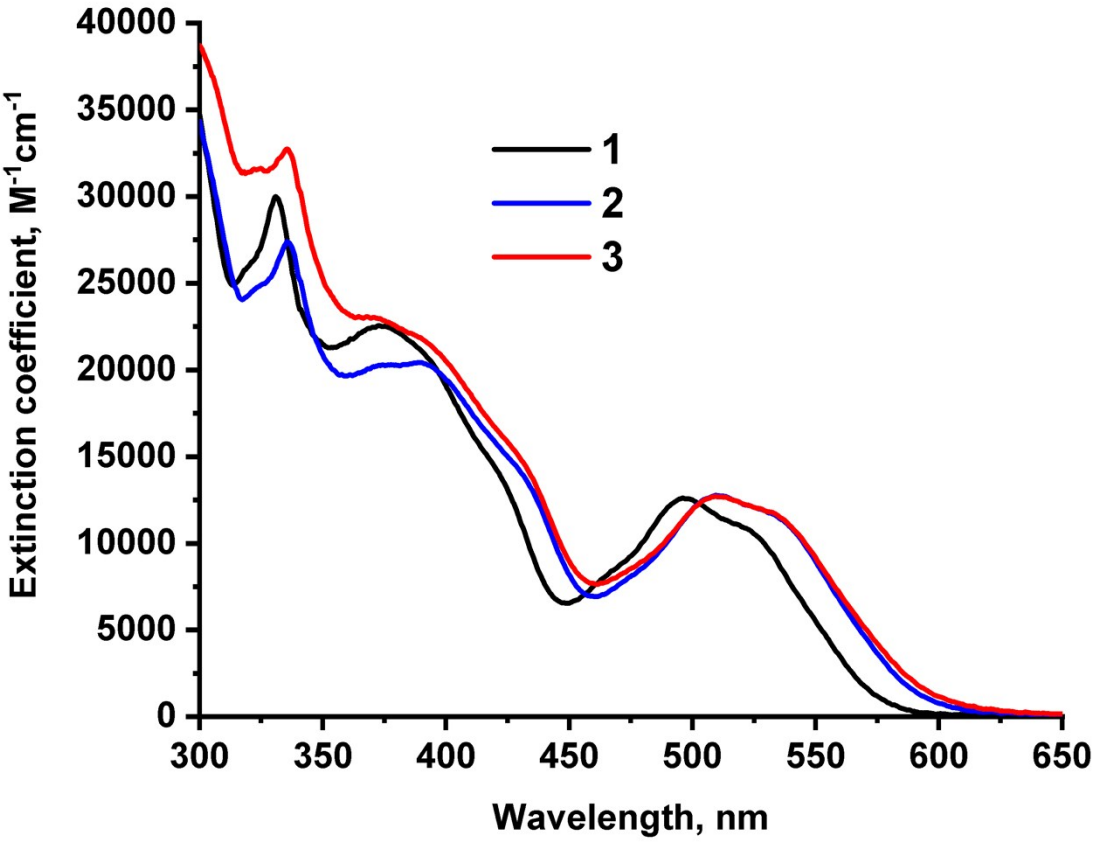

Figure S18A. Absorption spectra of **1-3** in MeOH solution at 298K.

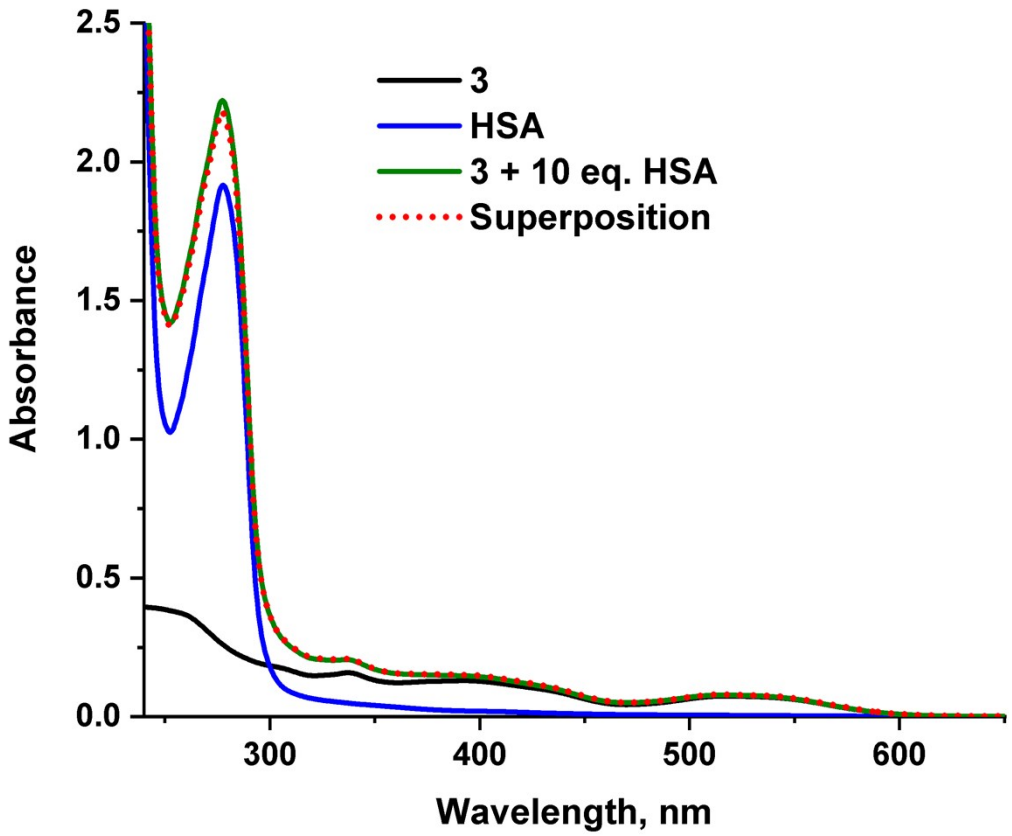

Figure S18B. Absorption spectra of **3** ($6*10^{-6}$ M), HSA ($6*10^{-5}$ M), mixture of **3** with 10 equivalents of HSA and superposition of **3** and HSA absorption spectra in 0.01M PBS aqueous solution at 298K.

Investigation of the non-covalent adducts of complexes 1 and 2 with HSA

Because of low solubility of **1** and **2** in water, it was quite natural to assume that these compounds form non-covalent adducts with human serum albumin (HSA) similar to their precursor **[Ir(N^C1)$_2$(N^N1)][PF$_6$],** and the analogs bearing the ligands with same aromatic systems but containing 1, 2, or 3 carboxyl groups at the complexes periphery.[1] Nevertheless, the question on the aggregates formation was unclear, since the complexes bearing OEG fragments are much better protected sterically and are more hydrophilic compared to their counterparts bearing carboxyl groups. Based on our previous findings, we may suppose that both these features should decrease HSA aggregation when the adducts are formed.[2] To clarify this issue, we prepared non-covalent adducts of **1** and **2** with HSA and investigated their molecular properties by Gel Permeation Chromatography (GPC).

The optimized protocol for preparation of the adducts was based on the procedure used earlier[1] to obtain the adducts with the **[Ir(N^C1)$_2$(N^N1)][PF$_6$]** complex as well as with the analogs bearing the ligands with same coordination core but containing 1, 2, or 3 auxiliary carboxyl groups. As in the case of carboxylic analogs, interaction of **1** and **2** with HSA gave some aggregation of the resulting adducts that provoked certain undesirable effects.

First, all these adducts displayed partial precipitation during further purification by dialysis. As a result, the adducts were centrifuged after preparation, dialyzed and freeze dried; thus we get rid of undesirable precipitate.

Second, GPC analysis of sedimentally stable adducts (prepared by direct dissolution of lyophilizates in water followed by centrifugation for 15 minutes at 10000 g) revealed the presence of aggregated species even after preparative centrifugation (Figure S19).

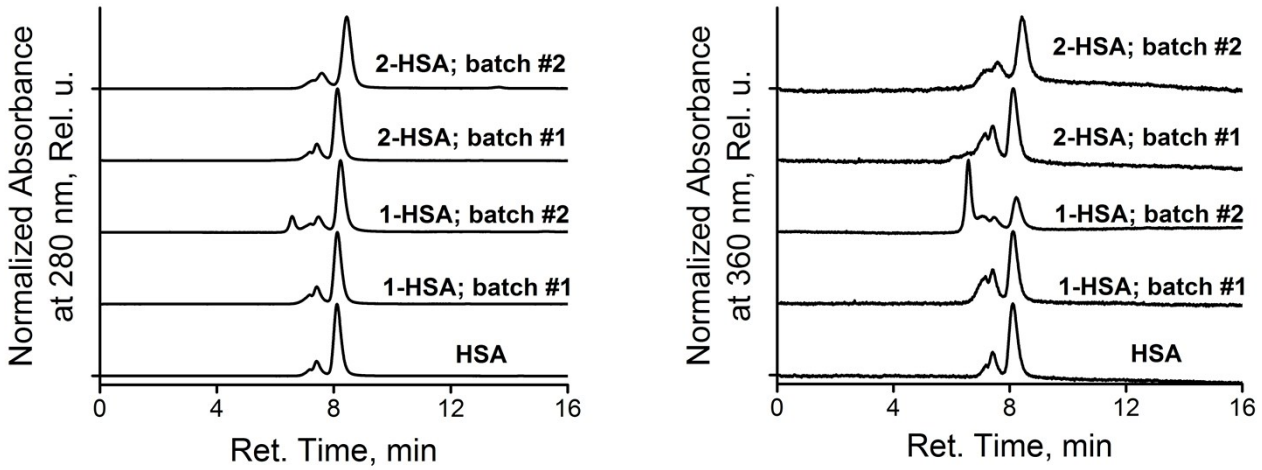

Figure S19. GPC traces of HSA and its adducts with complexes **1** and **2** recorded with UV detector at 280 (left) and 360 (right) nm.

This aggregation can be identified by the appearance of new chromatographic peaks in GPC traces in addition to those of parent HSA (the bottom traces in Figure 19), which displays three HSA fractions:[2] i) unimers, major peak with retention time (RT) from 7.8 to 8.6 min; ii) dimers, minor peak with RT from 7.3 to 7.8 min; iii) "oligomers", shoulder with RT from 6.8 to 7.3 min. The GPC traces of all these adducts demonstrate additional peaks that fall within the RT interval from 5.8 to 6.8 min and evidently correspond to larger and heavier species compared to those presented in the starting HSA. Unfortunately, the obtained adducts demonstrated substantial batch-to-batch variability in the number and shape of additional peaks (Figure S19). Nevertheless, it is clear that the HSA adducts with more hydrophobic complex **1-HSA** demonstrate more pronounced trend for aggregation as well as higher batch-to-batch variations in the aggregate composition (Figure S19), which is in full agreement with behavior of **[Ir(N^C1)$_2$(N^N1)][PF$_6$]**-HSA non-covalent adducts.[1] On the contrary, more hydrophilic (and better sterically protected) **2-HSA** revealed much lower tendency to aggregation. Partial irreproducibility of the aggregation is in line with our previous findings regarding non-covalent HSA adducts with hydrophobic organometallic complexes[1–4] and can be explained by several independent processes occurring simultaneously: formation of complexes precipitate germs stabilized by HSA shell that sterically or electrostatically protects them from macroscopic precipitation; aggregation of non-aggregated complex-HSA species because of incomplete burying of the complexes into HSA hydrophobic pockets, *etc.*[2] Moreover, as it was shown previously,[1,2] the higher hydrophobicity of parent complex the stronger propensity to precipitation and the larger portion of aggregated species can be obtained in less reproducible way.

Analysis of the data shown in Figure S19 indicates that the peaks of aggregates for all adducts studied are significantly stronger in the GPC traces recorded at 360 nm compared to those obtained at 280 nm.

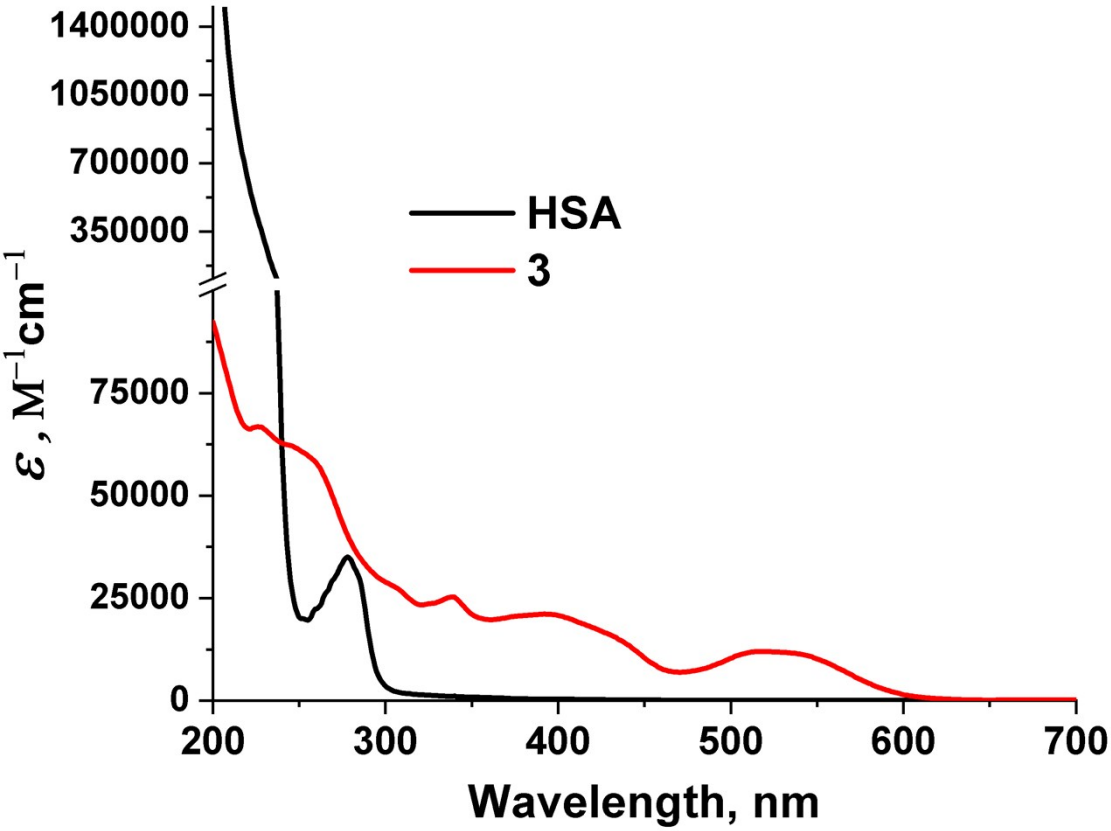

Figure S20. Molar extinction coefficients of HSA (black line) and **3** (red line).

Taking into account negligible adsorption of neat albumin at 360 nm and predominant contribution of the complexes at this wavelength (Figure S20) we can conclude that there is nonuniform distribution of the complexes between HSA unimers and aggregates with preferential location of iridium emitters in the latter species, as it was observer earlier for **[Ir(N^C1)$_2$(N^N1)][PF$_6$]** and its carboxylic analogs.[1]

Subcellular distribution of complex 3

For detailed analysis of intracellular localization of the complex **3**, CT26 cells were co-stained with commercial organelle probes (Thermo Fisher Scientific, England). Lysosomes were labeled with LysoTracker (3 μM for 1 h, excitation at 488 nm, detection at 500-600 nm); the Golgi complex was labeled with BODIPY FL C5-Ceramide (5 μM for 30 min, excitation at 488 nm, detection at 500-550 nm); mitochondria were identified by autofluorescence of NADH, nicotinamide adenine dinucleotide (two-photon excitation at 750 nm, detection at 450-500 nm). Nuclear DNA was labeled with DAPI (300 nM for 10 min, excitation at 405 nm, detection at 415-465 nm).

Manders' Overlap Coefficient was calculated in ZEN software (Carl Zeiss) and used as a measure of colocalization of organelle probes and complex 3. The values for the overlap coefficient range from 0 to 1, where a value of 1 represents perfectly colocalized pixels.

The results showed that complex **3** do not co-localize with nuclear DNA and cellular organelles such as lysosomes, the Golgi apparatus, and mitochondria (Figure S21, Table S1).

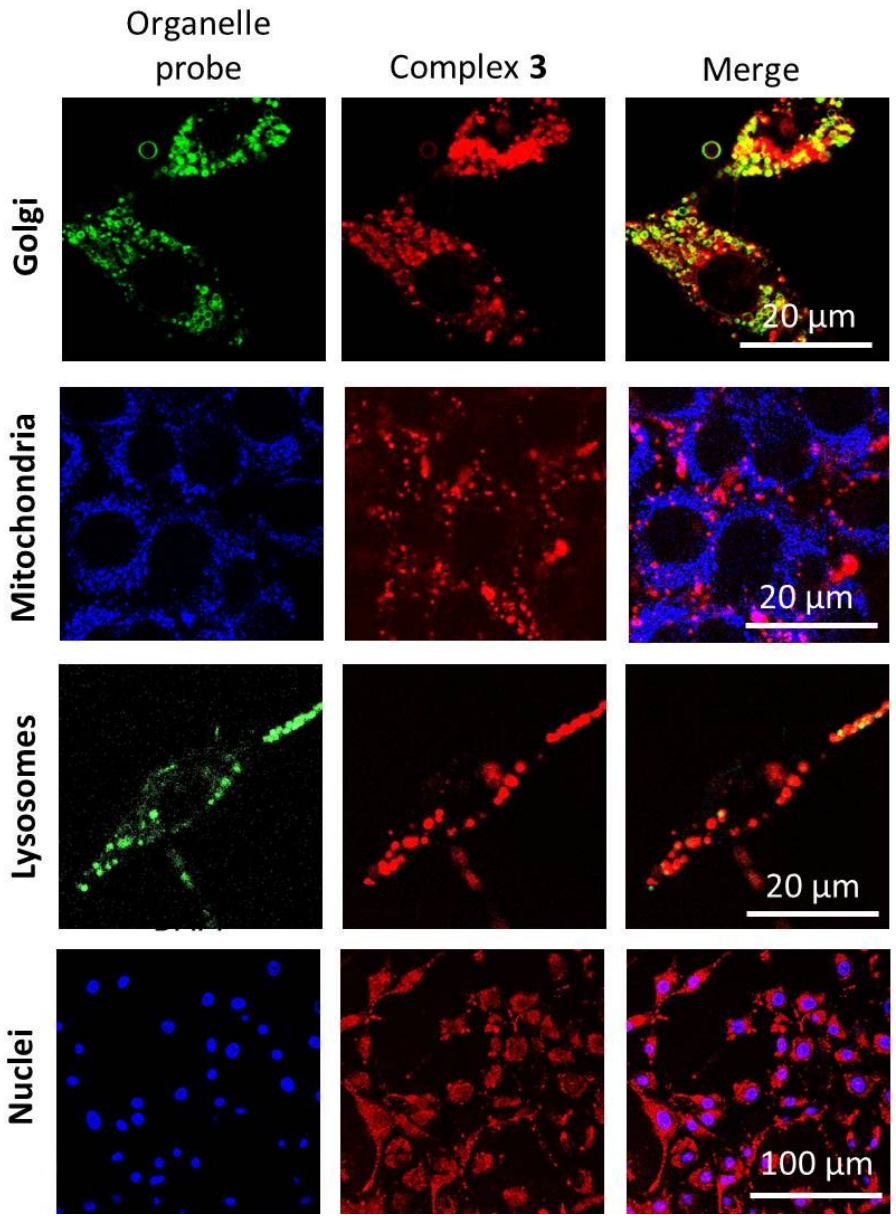

Figure S21. Subcellular distribution of complex **3** in mouse colorectal cancer cells CT26. Cells were co-stained with complex **3** and organelle-specific probes or DNA-binding dye DAPI. Laser scanning microscopy images of cells stained with the organelle probes, complex **3** and merged images are shown.

Table S1. Colocalization analysis for complex **3**. Mean±SD, n=15-20 cells.

	Golgi	**Mitochondria**	**Lysosomes**	**Nuclei**
The overlap coefficient	0.47±0.08	0.55±0.06	0.53±0.08	0.29±0.09

Supporting references

1 I. S. Kritchenkov, P. S. Chelushkin, V. V Sokolov, V. V Pavlovskiy, V. V Porsev, R. A. Evarestov and S. P. Tunik, *Organometallics*, 2019, **38**, 3740–3751.

2 A. I. Solomatina, V. A. Baigildin, D. D. Zhukovsky, D. V Krupenya, E. I. Koshel, V. I. Shcheslavskiy, S. P. Tunik and P. S. Chelushkin, *Colloid Polym. Sci.*, 2019, **297**, 325–337.

3 P. S. Chelushkin, N. V. Nukolova, A. S. Melnikov, P. Y. Serdobintsev, P. A. Melnikov, D. V. Krupenya, I. O. Koshevoy, S. V. Burov and S. P. Tunik, *J. Inorg. Biochem.*, 2015, **149**, 108–111.

4 P. S. Chelushkin, D. V. Krupenya, Y.-J. Tseng, T.-Y. Kuo, P.-T. Chou, I. O. Koshevoy, S. V. Burov and S. P. Tunik, *Chem. Commun.*, 2014, **50**, 849–851.